Proceedings of ALGORITMY 2012
pp. 393–403

THE LOCALIZED REDUCED BASIS MULTISCALE METHOD

FELIX ALBRECHT*, BERNARD HAASDONK†, SVEN KAULMANN† , AND MARIO OHLBERGER*

Abstract. In this paper we introduce the Localized Reduced Basis Multiscale (LRBMS) method for parameter dependent heterogeneous elliptic multiscale problems. The LRBMS method brings together ideas from both Reduced Basis methods to efficiently solve parametrized problems and from multiscale methods in order to deal with complex heterogeneities and large domains. Experiments on 2D and real world 3D data demonstrate the performance of the approach.

Key words. heterogeneous elliptic multiscale problems, numerical multiscale schemes, reduced basis methods, model order reduction, flow in porous media

AMS subject classifications. 35J20, 35B27, 65N30

1. Introduction. We are interested in efficiently simulating two-phase flow of two immiscible fluids (e.g., oil and water) in a porous medium $\Omega \subset \mathbb{R}^{d=2,3}$. The global pressure formulation for two-phase flow in porous media is given as follows. Given an end time $T \in \mathbb{R}^+$, find a global pressure $p : \Omega \times [0,T] \to \mathbb{R}$ and a phase saturation $s : \Omega \times [0,T] \to \mathbb{R}$, such that

$$-\nabla \cdot \big(\lambda(s) k \nabla p\big) = f \qquad \text{in } \Omega \times [0,T], \tag{1.1}$$

$$\Phi \partial_t s + \nabla \cdot \big(F_w(s, \nabla p)\big) - \nabla \cdot \big(D(s) \nabla s\big) = 0 \qquad \text{in } \Omega \times [0,T] \tag{1.2}$$

with suitable boundary and initial conditions. The permeability field $k \in L^\infty(\Omega)^{d \times d}$ may be complex heterogeneous for interesting domains. The total mobility is given by $\lambda(s) \in L^\infty(\Omega)$, depending smoothly on the saturation s. The convective flux F_w and the diffusive flux D involve the capillary pressure, the fractional flow rates and the phase mobilities (see [6] for details). Discretizing the above equations in time leads to a system, where an elliptic equation of type (1.1) has to be solved in each time step for different saturations s. Using standard methods this can become very costly, since a highly resolved discretization of (1.1) is required in each time step. In this paper we introduce the *Localized Reduced Basis Multiscale* (LRBMS) method to efficiently solve (1.1) for many saturations s and highly heterogeneous permeabilities k. Our approach follows the ideas from [8] with modifications concerning the underlying approximation spaces and a posteriori error estimates. It thereby combines ideas from reduced basis methods [11] with efficient numerical multiscale schemes as proposed in [1]. The LRBMS method allows us to efficiently and reliably approximate solutions of (1.1) for all time steps with the need to only solve (1.1) very few times. For a more detailed introduction to this model reduction approach for multiscale problems we refer to [9].

2. The Localized Reduced Basis Multiscale Method. Let $\Omega \subset \mathbb{R}^d$ be a connected domain with polygonal boundary $\partial\Omega = \Gamma_D \cup \Gamma_N$, where Γ_D and Γ_N with

*Institute of Computational and Applied Mathematics, University of Muenster, Einsteinstr. 62, 48149 Muenster, Germany ({felix.albrecht|mario.ohlberger}@uni-muenster.de).

†Institute of Applied Analysis and Numerical Simulation, University of Stuttgart, Pfaffenwaldring 57, 70569 Stuttgart, Germany ({sven.kaulmann|haasdonk}@mathematik.uni-stuttgart.de).

$\Gamma_D \cap \Gamma_N = \emptyset$ denote the Dirichlet and Neumann boundaries, respectively. Let further $\mathcal{P} \subset \mathbb{R}^p$ denote a bounded set of possible parameters and $\boldsymbol{\mu}, \overline{\boldsymbol{\mu}} \in \mathcal{P}$ parameter vectors. As motivated in the introduction, the elliptic equation (1.1) will serve as our model problem. To be more precise, we allow the data functions $\lambda(x;\boldsymbol{\mu})$ and $f(x;\boldsymbol{\mu})$ to be parameter dependent and we assume suitable parameter dependent Dirichlet and Neumann values $g_D(x;\boldsymbol{\mu})$ and $g_N(x;\boldsymbol{\mu})$, respectively. The symbol $n_\Omega \in \mathbb{R}^d$ will denote the unit outward normal to Ω.

2.1. Fine scale Discontinuous Galerkin approximation. We discretize the elliptic problem by an Interior Penalty Discontinuous Galerkin (DG) method [3]. This fine scale approximation will provide the reference solution for our method as well as snapshots that are used to generate the basis of our coarse approximation space. Let τ_h be an admissible triangulation of Ω with codim 0 entities $t \in \tau_h$ *(elements)* and grid width $h := \max_{t\in\tau_h} \operatorname{diam}(t)$. We call τ_h a *fine triangulation*. We denote the set of codim 1 entities *(facets)* which lie on Γ_D by ε_D, the set of facets which lie on Γ_N by ε_N and the set of facets which do not lie on $\partial\Omega$ by ε_I. We also denote the width of a facet $e \in \varepsilon_I \cup \varepsilon_D \cup \varepsilon_N$ by $h_e := \operatorname{diam}(e)$. We call a facet $e \in \varepsilon_I$ *inner facet* and a facet $e \in e_D \cup e_N$ *boundary facet*. On τ_h we define the fine DG space $\mathcal{V}_h^k := \left\{ v \in L^2(\Omega) \middle| v|_t \in \mathbb{P}_k(t) \quad \forall t \in \tau_h \right\}$, where $\mathbb{P}_k$ denotes the space of polynomials of degree at most $k \in \mathbb{N}_0$. Since $\mathcal{V}_h^k \not\subset H^1(\Omega)$ we have a non-conforming discretization, and functions $v \in \mathcal{V}_h^k$ are two-valued on inner facets. For $v \in \mathcal{V}_h^k$ we define its jump by $[\![v]\!] := v|_t - v|_s$ and its mean by $\{\!\{v\}\!\} := \frac{1}{2}(v|_t + v|_s)$ on an inner facet $e = t \cap s \in \varepsilon_I$ and by $[\![v]\!] := v$ and $\{\!\{v\}\!\} := v$ on a boundary facet, respectively. Note, that for all inner facets $e = t \cap s$, we assume a prescribed order of the elements t and s, such that the definition of the jump and the facets normal $n_e \in \mathbb{R}^d$ is well-defined. Let $b_h : \mathcal{V}_h^1 \times \mathcal{V}_h^1 \times \mathcal{P} \to \mathbb{R}$ and $l_h : \mathcal{V}_h^1 \times \mathcal{P}$ denote the Interior Penalty DG bilinear form and linear functional respectively, given by

$$
\begin{aligned}
b_h(u,v;\boldsymbol{\mu}) :=& \sum_{t\in\tau_h} \int_t \lambda(\boldsymbol{\mu}) k \nabla u \cdot \nabla v \,\mathrm{dx} + \sum_{e\in\varepsilon_I\cup\varepsilon_D} \int_e \tfrac{\sigma_e(\lambda(\boldsymbol{\mu}),k)}{h_e} [\![u]\!]\,[\![v]\!]\,\mathrm{ds}, \\
&- \sum_{e\in\varepsilon_I\cup\varepsilon_D} \left[\int_e \{\!\{\lambda(\boldsymbol{\mu}) k \nabla u \cdot n_e\}\!\}\,[\![v]\!]\,\mathrm{ds} + \int_e \{\!\{\lambda(\boldsymbol{\mu}) k \nabla v \cdot n_e\}\!\}\,[\![u]\!]\,\mathrm{ds} \right] \\
l_h(v;\boldsymbol{\mu}) :=& \sum_{t\in\tau_h} \int_t f(\boldsymbol{\mu}) v \,\mathrm{dx} \\
&+ \sum_{e\in\varepsilon_D} \int_e \left(\tfrac{\sigma_e(\lambda(\boldsymbol{\mu}),k)}{h_e} v - \lambda(\boldsymbol{\mu}) k \nabla v \cdot n_e \right) g_D(\boldsymbol{\mu})\,\mathrm{ds} + \sum_{e\in\varepsilon_N} \int_e g_N(\boldsymbol{\mu}) v \,\mathrm{ds},
\end{aligned}
$$

where the local penalty function $\sigma_e : \Omega \to \mathbb{R}^+$ is chosen constant free and linear with respect to its first argument as proposed in [2].

Definition 2.1 (Fine scale Discontinuous Galerkin approximation). *Given a parameter $\boldsymbol{\mu} \in \mathcal{P}$, determine $p_h(\boldsymbol{\mu}) \in \mathcal{V}_h^1$ such that*

$$
b_h(p_h(\boldsymbol{\mu}), v_h; \boldsymbol{\mu}) = l_h(v_h;\boldsymbol{\mu}) \qquad \text{for all } v_h \in \mathcal{V}_h^1. \tag{2.1}
$$

Problem (2.1) has a unique solution by the Lax-Milgram theorem since b_h is continuous and coercive and l_h is continuous and bounded if the data functions and the local penalty function are chosen accordingly [3].

2.2. Coarse scale Reduced Basis approximation. The main idea of our method is to introduce a so called *reduced broken space* $\mathcal{W}_N \subset \mathcal{V}_h^k$ which is associated with a coarse triangulation $\mathcal{T}_H$ of Ω and spanned by local basis function. These local basis functions can for instance be obtained by localizing solutions of (2.1) to the individual elements of the coarse triangulation. Due to these basis functions the reduced broken space incorporates the features of the fine scale while being of much lower dimension than the fine DG space. Given a fine triangulation τ_h let $\mathcal{T}_H$ be a coarse triangulation. By this we mean that elements $T \in \mathcal{T}_H$ are each made up of a connected set of fine elements $t \in \tau_h^T := \tau_h \cap T$, in such a way, that each fine element $t \in \tau_h$ lies inside exactly one coarse element $T \in \mathcal{T}_H$. We introduce $H := \max_{T\in\mathcal{T}_H} \operatorname{diam}(T)$ to denote the grid width of $\mathcal{T}_H$. Given a local basis $\Phi^T := \{\varphi_1^T, \dots, \varphi_{N^T}^T\}$ of $N^T \in \mathbb{N}$ basis functions φ_i^T with $\operatorname{supp}(\varphi_i^T) \subseteq T$ for all $1 \le i \le N^T$ on each coarse element $T \in \mathcal{T}_H$ we define the *local reduced spaces* $\mathcal{W}_{N^T}^T \subset L^2(T)$ by $\mathcal{W}_{N^T}^T := \operatorname{span}(\Phi^T)$ for all $T \in \mathcal{T}_H$ and the *reduced broken space* $\mathcal{W}_N \subset \mathcal{V}_h^k$ by $\mathcal{W}_N := \operatorname{span}(\bigcup_{T\in\mathcal{T}_H} \mathcal{W}_{N^T}^T)$ with dimension $N := \sum_{T\in\mathcal{T}_H} N^T$.

Definition 2.2 (Localized Reduced Basis Multiscale approximation). *Given b_h and and l_h as in Definition 2.1 the Localized Reduced Basis Multiscale approximation of our problem reads: Given a parameter $\boldsymbol{\mu} \in \mathcal{P}$, determine $p_N(\boldsymbol{\mu}) \in \mathcal{W}_N$, such that*

$$b_h(p_N(\boldsymbol{\mu}), v_N; \boldsymbol{\mu}) = l_h(v_N; \boldsymbol{\mu}) \qquad \text{for all } v_N \in \mathcal{W}_N.$$

3. A posteriori error analysis. We will now present an efficient residual based a posteriori estimate for the error between the LRBMS approximation and the fine DG approximation in the energy norm induced by b_h. The following derivations are an instantiation of the general RB framework, e.g. presented in [11]. For our analysis and the offline/online decomposition of the LRBMS approximation (see Section 4) we assume b_h and l_h to be parameter separable, i.e.

$$b_h(u, v; \boldsymbol{\mu}) = \sum_{q=1}^{Q_b} \Theta_b^q(\boldsymbol{\mu}) b_h^q(u, v) \qquad \text{and} \qquad l_h(v; \boldsymbol{\mu}) = \sum_{q=1}^{Q_l} \Theta_l^q(\boldsymbol{\mu}) l_h^q(v), \tag{3.1}$$

where $\Theta_b^q, \Theta_l^q : \mathcal{P} \to \mathbb{R}^+$ denote the $Q_b \in \mathbb{N}$ and $Q_l \in \mathbb{N}$ coefficients of b_h and l_h and $b_h^q : \mathcal{V}_h^k \times \mathcal{V}_h^k \to \mathbb{R}$ and $l_h^q : \mathcal{V}_h^k \to \mathbb{R}$ denote the parameter independent components of b_h and l_h, respectively. This assumption can be satisfied by considering correspondingly separable data functions. In the more general case of non-separable parametric data functions and possibly nonlinear b_h and l_h a similar approximate decomposition can be achieved by applying the Empirical Interpolation technique [4, 7].

Definition 3.1 (Energy scalar product and norm). *For a given parameter $\boldsymbol{\mu} \in \mathcal{P}$ we define the energy scalar product $(\cdot,\cdot)_{\boldsymbol{\mu}} : \mathcal{V}_h^k \times \mathcal{V}_h^k \to \mathbb{R}$ and its induced energy norm $\|\cdot\|_{\boldsymbol{\mu}} : \mathcal{V}_h^k \to \mathbb{R}^+$ by*

$$(u, v)_{\boldsymbol{\mu}} := b_h(u, v; \boldsymbol{\mu}) \qquad \text{and} \qquad \|u\|_{\boldsymbol{\mu}} := \sqrt{(u, u)_{\boldsymbol{\mu}}}. \tag{3.2}$$

For parameters $\boldsymbol{\mu}, \overline{\boldsymbol{\mu}} \in \mathcal{P}$ the norms $\|\cdot\|_{\boldsymbol{\mu}}$ and $\|\cdot\|_{\overline{\boldsymbol{\mu}}}$ are equivalent in the sense that

$$\sqrt{\alpha_{\overline{\boldsymbol{\mu}}}(\boldsymbol{\mu})}\|u\|_{\overline{\boldsymbol{\mu}}} \quad \le \quad \|u\|_{\boldsymbol{\mu}} \quad \le \quad \sqrt{\gamma_{\overline{\boldsymbol{\mu}}}(\boldsymbol{\mu})}\|u\|_{\overline{\boldsymbol{\mu}}} \tag{3.3}$$

for all $u \in \mathcal{V}_h^k$, *where* $\alpha_{\overline{\boldsymbol{\mu}}}(\boldsymbol{\mu}), \gamma_{\overline{\boldsymbol{\mu}}}(\boldsymbol{\mu}) : \mathcal{P} \to \mathbb{R}^+$ *are given by*

$$\alpha_{\overline{\boldsymbol{\mu}}}(\boldsymbol{\mu}) := \min_{q=1}^{Q_b} \frac{\Theta_b^q(\boldsymbol{\mu})}{\Theta_b^q(\overline{\boldsymbol{\mu}})} \qquad \textit{and} \qquad \gamma_{\overline{\boldsymbol{\mu}}}(\boldsymbol{\mu}) := \max_{q=1}^{Q_b} \frac{\Theta_b^q(\boldsymbol{\mu})}{\Theta_b^q(\overline{\boldsymbol{\mu}})}. \tag{3.4}$$

The norm equivalence (3.3) is obtained by combining the definition of the energy norm (3.2) and the decomposition of b_h (3.1). The constant $\alpha_{\overline{\boldsymbol{\mu}}}$ is evaluated using the so-called min $-\theta$ approach [11].

For the RB error analysis we introduce the residual and its Riesz-representative. For a given function $u \in \mathcal{V}_h^k$ let the *residual* $r_h[u] : \mathcal{V}_h^k \times \mathcal{P} \to \mathbb{R}$ be given by

$$r_h[u](v; \boldsymbol{\mu}) := l_h(v; \boldsymbol{\mu}) - b_h(u, v; \boldsymbol{\mu}) \qquad \text{for all } v \in \mathcal{V}_h^k$$

and its *Riesz-representative* $r_u(\boldsymbol{\mu}) \in \mathcal{V}_h^k$, given a parameter $\overline{\boldsymbol{\mu}} \in \mathcal{P}$, such that

$$(r_u(\boldsymbol{\mu}), v)_{\overline{\boldsymbol{\mu}}} = r_h[u](v; \boldsymbol{\mu}) \qquad \text{for all } v \in \mathcal{V}_h^k. \tag{3.5}$$

The energy norm of the residual serves as the actual error estimator:

THEOREM 3.2 (Residual based a posteriori error estimate). *Given parameters* $\boldsymbol{\mu}, \overline{\boldsymbol{\mu}} \in \mathcal{P}$ *the energy norm of the Riesz-representative to a given LRBMS approximation* $p_N(\boldsymbol{\mu})$ *is an efficient a posteriori error estimate in the sense that*

$$\tfrac{1}{\sqrt{\gamma_{\overline{\boldsymbol{\mu}}}(\boldsymbol{\mu})}} \left\| r_{p_N(\boldsymbol{\mu})}(\boldsymbol{\mu}) \right\|_{\overline{\boldsymbol{\mu}}} \quad \leq \quad \| p_h(\boldsymbol{\mu}) - p_N(\boldsymbol{\mu}) \|_{\overline{\boldsymbol{\mu}}} \quad \leq \quad \tfrac{1}{\sqrt{\alpha_{\overline{\boldsymbol{\mu}}}(\boldsymbol{\mu})}} \left\| r_{p_N(\boldsymbol{\mu})}(\boldsymbol{\mu}) \right\|_{\overline{\boldsymbol{\mu}}}.$$

Proof. Both inequalities are obtained by using the definition of the energy norm (3.2), the error identity $b_h(e_h(\boldsymbol{\mu}), v; \boldsymbol{\mu}) = r_h[p_N(\boldsymbol{\mu})](v; \boldsymbol{\mu})$ for all $v \in \mathcal{V}_h^k$, the definition of the Riesz-representative (3.5), the Cauchy-Schwarz inequality and the norm equivalence (3.3). □

4. Offline/online decomposition. One of the key benefits of our method is the fact that we precompute all parameter independent quantities in a preparatory offline step, which is of polynomial order in $\dim(\mathcal{V}_h^k)$. During the online phase of the simulation, a LRBMS approximation is then quickly obtained in complexity polynomial in $\dim(\mathcal{W}_N)$ which is independent of h. This holds true also for the evaluation of the error estimator.

During the offline-phase, we determine a basis $\Phi^N = \{\varphi_1, \ldots, \varphi_N\}$ of $\mathcal{W}_N$ (see Definition 5.1 for a possible choice of Φ^N) and then proceed as in stationary elliptic RB methods [11]. We precompute the parameter independent Gram-matrices $\underline{b}^q \in \mathbb{R}^{N \times N}$ for each component of b_h and the reduced vectors $\underline{l}^q \in \mathbb{R}^N$ for each component of l_h, given by $(\underline{b}^q)_{i,j} := b_h^q(\varphi_i, \varphi_j)$ for all $1 \leq i, j \leq N$ and $1 \leq q \leq Q_b$ and $(\underline{l}^q)_j := l_h^q(\varphi_j)$ for all $1 \leq j \leq N$ and $1 \leq q \leq Q_l$. It is worth noting that since the basis functions φ_i have a local support the computation of the above quantities is only of order τ_h^T and can in addition be easily parallelized. In the online-phase, given a parameter $\boldsymbol{\mu} \in \mathcal{P}$, we obtain the reduced system matrix $\underline{b(\boldsymbol{\mu})} \in \mathbb{R}^{N \times N}$ and the reduced right hand side $\underline{l(\boldsymbol{\mu})} \in \mathbb{R}^N$ by $\underline{b(\boldsymbol{\mu})} = \sum_{q=1}^{Q_b} \Theta_b^q(\boldsymbol{\mu}) \underline{b}^q$ and $\underline{l_h(\boldsymbol{\mu})} = \sum_{q=1}^{Q_l} \Theta_l^q(\boldsymbol{\mu}) \underline{l}^q$ and the reduced vector of Degrees of Freedom (DoF) $\underline{p(\boldsymbol{\mu})} \in \mathbb{R}^N$ as the solution of $\underline{b(\boldsymbol{\mu})} \cdot \underline{p(\boldsymbol{\mu})} = \underline{l(\boldsymbol{\mu})}$ with a computational complexity independent of h.

We derive a similar decomposition of the Riesz-representative for any function $u = \sum_{i=1}^N u_i \varphi_i \in \mathcal{W}_N$ using (3.5), $r_u(\boldsymbol{\mu}) = \sum_{q=1}^{Q_r} \Theta_r^q(\boldsymbol{\mu}) r_h^q$, where the coefficients Θ_r^q

depend on the coefficients of b_h and l_h and the DoFs u_i and the components r_h^q are solutions to problems of type

$$(r_h^q, v_h)_{\overline{\boldsymbol{\mu}}} = l_h^j(v_h), \quad \text{or} \quad (r_h^q, v_h)_{\overline{\boldsymbol{\mu}}} = b_h^j(\varphi_i, v_h), \quad \text{for all } v_h \in \mathcal{V}_h^k$$

for all combinations of $1 \leq i \leq N$ and $1 \leq j \leq Q_b, Q_l$. In the offline-phase we precompute these parameter independent components r_h^q for all $1 \leq q \leq Q_r$ as well as the Gram-matrix $\underline{g} \in \mathbb{R}^{Q_r \times Q_r}$, given by $\big(\underline{g}\big)_{i,j} := b_h(r_h^i, r_h^j; \overline{\boldsymbol{\mu}})$. It is worth noting that, again, these computations are completely independent of each other and can thus be easily parallelized. Given a parameter $\boldsymbol{\mu} \in \mathcal{P}$ and a LRBMS approximation $p_N(\boldsymbol{\mu}) \in \mathcal{W}_N$ we compute the constants $\alpha_{\overline{\boldsymbol{\mu}}}(\boldsymbol{\mu}), \gamma_{\overline{\boldsymbol{\mu}}}(\boldsymbol{\mu}) \in \mathbb{R}$ from (3.4) and the coefficient vector $\underline{\Theta_r(\boldsymbol{\mu})} \in \mathbb{R}^{Q_r}$, given by $\big(\underline{\Theta_r(\boldsymbol{\mu})}\big)_j := \Theta_r^j(\boldsymbol{\mu})$ for all $1 \leq j \leq Q_r$, to obtain the error estimator with a computational complexity independent of h: $\big\|r_{p_N(\boldsymbol{\mu})}(\boldsymbol{\mu})\big\|_{\overline{\boldsymbol{\mu}}} = \sqrt{\underline{\Theta_r(\boldsymbol{\mu})}^t \, \underline{g} \, \underline{\Theta_r(\boldsymbol{\mu})}}$.

5. Numerical experiments. In our experiments we obtain the reduced broken space $\mathcal{W}_N$ by the following algorithm combining a localized variant of the Greedy algorithm [12] with a final compression step by a principal component analysis (PCA) analog to [8].

DEFINITION 5.1 (Localized Greedy). *Given a finite set of training parameters $\mathcal{S} \subset \mathcal{P}$, a maximum basis size $N_{max} \in \mathbb{N}$, an error tolerance $\Delta_{error} \in \mathbb{R}^+$ and a PCA tolerance $\Delta_{PCA} \in \mathbb{R}^+$, the following algorithm produces a reduced broken space $\mathcal{W}_N$:*

(i) Pick a parameter $\boldsymbol{\mu}_0 \in \mathcal{S}$ and initialize the local bases by $\Phi_{(0)}^T := \emptyset$ and set $N_{(0)}^T = 0$ for all $T \in \mathcal{T}_H$ and $k = 1$.

(ii) Given local bases $\Phi_{(k-1)}^T$ of size $N_{(k-1)}^T \in \mathbb{N}$ for all $T \in \mathcal{T}_H$ and a parameter $\boldsymbol{\mu}_{k-1} \in \mathcal{S}$, compute a global fine DG snapshot $p_h(\boldsymbol{\mu}_{k-1}) \in \mathcal{V}_h^k$ and set the extended local bases as $\Phi_{(k)}^T := \Phi_{(k-1)}^T \cup \{p_h(\boldsymbol{\mu}_{k-1})\big|_T\}$ with size $N_{(k)}^T := N_{(k-1)}^T + 1$ for all $T \in \mathcal{T}_H$. Set the global basis as $\Phi_{(k)} := \bigcup_{T \in \mathcal{T}_H} \Phi_{(k)}^T$ of size $N_{(k)} := \sum_{T \in \mathcal{T}_H} N_{(k)}^T$ and compute all offline quantities for this basis.

(iii) Compute LRBMS approximations $p_N(\boldsymbol{\mu}) \in \mathcal{W}_{N_{(k)}}$ for all training parameters $\boldsymbol{\mu} \in \mathcal{S}$ using the current basis and evaluate the error estimator to find the parameter $\boldsymbol{\mu}_{(k)} \in \mathcal{S}$ which maximizes the error estimator.

(iv) IF $N_{(k)} < N_{max}$ and if the estimated error for $p_N(\boldsymbol{\mu}_{(k)})$ is larger than Δ_{error}:
Set $k := k + 1$ and repeat from (ii).
ELSE:
Apply the PCA to $\Phi_{(k)}^T$ with tolerance Δ_{PCA} on each $T \in \mathcal{T}_H$ to obtain the localized orthogonalized reduced bases Φ^T of size $N^T \leq N_{(k)}^T$ on each $T \in \mathcal{T}_H$.

(v) Set the global basis as $\Phi := \bigcup_{T \in \mathcal{T}_H} \Phi^T$ of size $N_\cdot = \sum_{T \in \mathcal{T}_H} N^T$ and compute all offline quantities for this basis.

In the following we will demonstrate the performance of our approach using two different examples which fit in the framework of our elliptic problem. The first example, the 2D thermal block example, is easily scalable concerning parameter and spatial complexity and is therefore well-suited to highlight the basic principle of our method: The scaling between offline and online cost. The second example is much closer to real-world applications: Here we use 3D real-world data taken from the SPE10 benchmark problem [10], putting our method in the context of two-phase flow equations and multiscale problems. All implementations are realized within the software framework

DUNE [5].

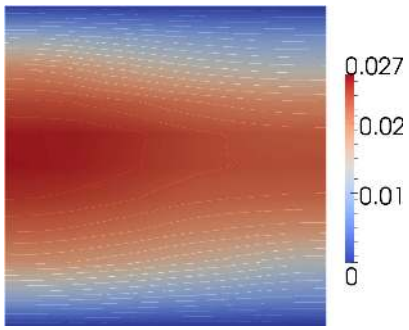

FIG. 5.1. *Solution of the thermalblock problem with isolines for* $\boldsymbol{\mu} = (3, 6, 9, 2, 5, 8, 1, 4, 7, 10, 3, 6, 9, 2, 5, 8)'$.

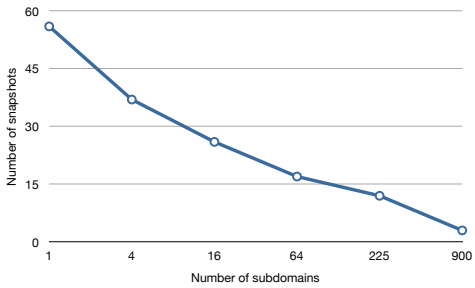

FIG. 5.2. *Number of snapshots needed against number of subdomains during the generation of the reduced basis with the Greedy algorithm for different coarse triangulations*

5.1. The Thermal Block Example. In this example, we solve (1.1) on $\Omega = [0,1]^2$ with a constant permeability $k \equiv 1$ and a parameter-dependent mobility given by $\lambda(\boldsymbol{\mu}) = \sum_{q=1}^{Q_\lambda} \Theta_\lambda^q(\boldsymbol{\mu}) \chi_{\Omega_q}$, where $\chi_{\Omega_q} : \Omega \to \{0,1\}$ are characteristic functions for the $Q_\lambda \in \mathbb{N}^{\geq 1}$ blocks $\Omega_q \subset \Omega$ with $Q_q \cap Q_s = \emptyset$ for $q \neq s$. These blocks are given by an equidistant triangulation of Ω into $Q_\lambda = 4 \cdot 4 = 16$ square elements. The coefficients $\Theta_\lambda^q(\boldsymbol{\mu})$ for $1 \leq q \leq Q_\lambda$ are given by $\Theta_\lambda^q(\boldsymbol{\mu}) = \boldsymbol{\mu}_q$ for $\boldsymbol{\mu}_q \in [0.1, 10]$. Choosing $f(\boldsymbol{\mu}) \equiv 1$, $\Gamma_D = [0,1] \times \{0\} \cup [0,1] \times \{1\}$, $\Gamma_N = \partial\Omega \setminus \Gamma_D$, $g_D(\boldsymbol{\mu}) \equiv 0$ and $g_N(\boldsymbol{\mu}) \equiv 0$, the description of the problem setting is complete. We discretized this problem using a rectangular grid with $30 \cdot 30 = 900$ fine grid elements and applied our method using rectangular coarse triangulations with $1, 2 \cdot 2, 4 \cdot 4, 8 \cdot 8, 15 \cdot 15$ and $30 \cdot 30$ coarse grid elements (*subdomains*). We ran the Greedy algorithm with a tolerance of $\Delta_{\text{error}} = 0.05$ for the estimated absolute error over the training set which consisted of 100 randomized parameters in the above-mentioned parameter domain. The training set consisted of the same random parameters for all basis generation procedures. A typical fine DG solution is plotted in Figure 5.1.

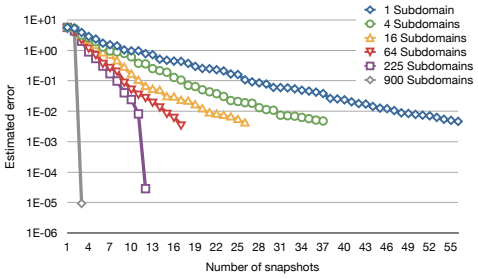

FIG. 5.3. *Maximum estimated absolute error over training set against number of snapshots needed during Greedy algorithm for different sizes of the coarse triangulation.*

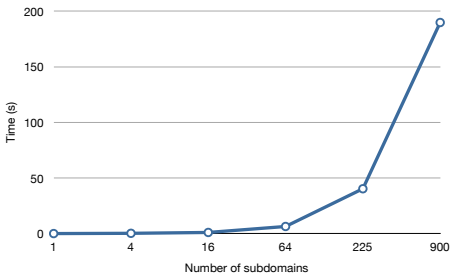

FIG. 5.4. *Time needed to update the error estimator during the Greedy algorithm: Mean over all steps in seconds against number of subdomains for different coarse triangulations.*

Figure 5.2 shows the number of total snapshots needed during the Greedy algorithm to fulfill the error tolerance for different sizes of the coarse triangulation. We

see that we are able to scale the offline cost in terms of needed snapshots by choosing different coarse triangulations. The number of snapshots ranges from 56 for one coarse grid element (which corresponds to a standard RB method) to only three snapshots for 900 coarse grid elements. The latter is the expected behavior since three linearly independent functions on each element are sufficient to represent a linear function in two spatial dimensions. This scaling quality of our approach can also be seen in Figure 5.3 where we demonstrate the evolution of the maximum estimated absolute error over the training set during the offline procedure. We see how with an increasing number of coarse elements the error decent gets steeper.

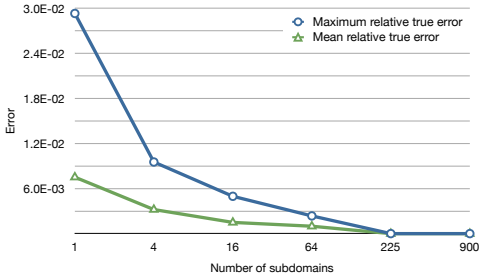

FIG. 5.5. *Maximum and mean relative true error in the energy norm over the test set for different coarse triangulations.*

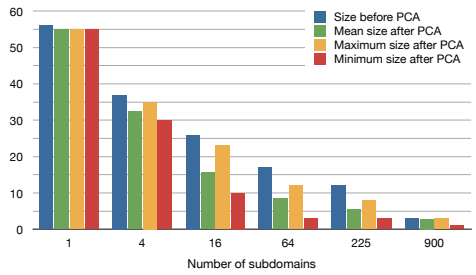

FIG. 5.6. *Mean, maximal and minimal number of local basis functions on the different coarse grids before and after the PCA.*

Clearly these qualities come with additional costs: With increasing size of the coarse grid, the update of the error estimator becomes more and more costly as we have to solve the high-dimensional equation once for every new basis function on every coarse element. This increase in the offline cost can be seen in Figure 5.4, where we compare the mean estimator update time for the different coarse triangulations. As the computations of the Riesz-representatives are independent of each other, this step can be easily parallelized. Thus it should be possible to compensate for the additional costs by increasing the number of used CPUs with increasing coarse grid size. For the experiments at hand we used a shared memory parallelization which needs to be further improved by more sophisticated parallelization techniques as our approach is obviously not able to fully compensate for the additional costs.

Similar to the update time for the error estimator, the total training time (time for reduced simulations and estimator evaluations for all training parameters during the offline phase) increases with increasing coarse grid sizes as the reduced basis Φ grows a lot faster (than the basis of the standard RB method) during the Greedy algorithm. Nevertheless, since we aim at applications with extremely costly detailed simulations, this increase is usually negligible.

Furthermore, our localized method has another nice quality: The online error over a given fixed test set decreases with increasing numbers of coarse elements. This is due to the greater flexibility in the reduced scheme with our method. This phenomenon can be seen in Figure 5.5 where the maximum relative true error in the energy norm over the test set drops from 0.03 for 1 subdomain to 0.002 for 64 subdomains and finally to $7 \cdot 10^{-12}$ for 900 subdomains.

Finally, in Figure 5.6 we see the effect of the PCA. As described in Definition 5.1 we applied the PCA on each coarse element, using a tolerance of $\Delta_{\mathrm{PCA}} = 1 \cdot 10^{-7}$. We see that, up to a certain point, refinements of the coarse grid lead to bigger differences

between maximum and minimum basis sizes. This behavior is expected as finer coarse triangulations lead to a greater resemblance of the snapshots on each coarse element (in particular in regions, where the snapshots do not differ too much, for example close to the Dirichlet boundaries). Beginning with a coarse grid size of about 225, this effect starts to vanish as the bases on the coarse elements get more and more compact and therefore the possibility for reduction with the PCA vanishes. Also remarkable is the fact that the PCA reduces the standard Greedy basis (which corresponds to 1 subdomain in Figure 5.6) only by one function. On one coarse element the Greedy algorithm seems to work as good as the PCA: The basis is already very compact.

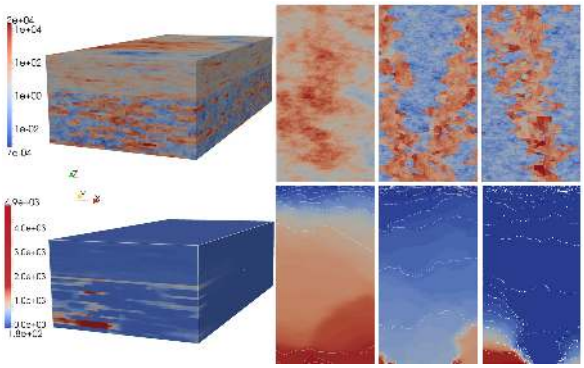

FIG. 5.7. *Permeability field (top) and solution (bottom) of the SPE10 problem for* $\boldsymbol{\mu} = (0.01, 0.01, 0.95, 0.01, 0.01, 0.01)'$. *Left: Whole field, z-axis scaled by 4. Right: Cuts along the x-y-plane at different values of z, demonstrating the channel structures in the permeability and matching solution with isolines (bottom).*

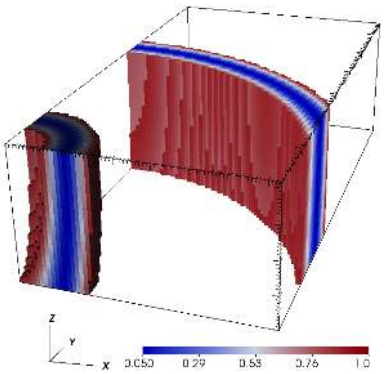

FIG. 5.8. *Threshold plot (values between 0 and 0.9) of mobility for* $\boldsymbol{\mu} = (0.01, 0.95, 0.01, 0.01, 0.01, 0.01)'$ *and* $\boldsymbol{\mu} = (0.01, 0.01, 0.01, 0.01, 0.01, 0.95)'$ *(front and back). Z-axis scaled by 4.*

5.2. The SPE10 Example. The second example uses real-world data taken from the SPE10 benchmark problem [10]. The goal of this benchmark problem was to compare different upscaling techniques for two-phase flow problems as motivated in section 1. In this example we use the permeability field given in the SPE10 benchmark and a mobility function that models the flooding of the domain by one of the phases to solve (1.1) on $\Omega = [0, 365.76] \times [0, 670.56] \times [0, 51.816]$. The fine triangulation of Ω consists of $60 \cdot 220 \cdot 42 = 554400$ cubes. The permeability field is displayed in Figure 5.7 (top).

For a given center $x_0 \in \mathbb{R}^3$, a given transition width $\varepsilon \in \mathbb{R}^{>0}$ and $Q_\lambda \in \mathbb{N}^{\geq 1}$ radii $\alpha_q \in \mathbb{R}^{>0}$ for $1 \leq q \leq Q_\lambda$ the mobility is given by $\lambda(x, \boldsymbol{\mu}) = \sum_{q=1}^{Q_\lambda} \Theta_\lambda^q(\boldsymbol{\mu}) \lambda_q(x)$ with components $\lambda_q(x) = 1 - \chi_{B_{\alpha_q+\varepsilon}(x_0)}(x) \cdot (1 - \chi_{B_{\alpha_q-\varepsilon}(x_0)}(x)) \cdot \sin^2\left(\pi \frac{|x-x_0|+\varepsilon-\alpha_q}{2\varepsilon}\right)$ and coefficients $\Theta_\lambda^q(\boldsymbol{\mu}) = \boldsymbol{\mu}_q$ for $1 \leq q \leq Q_\lambda$. We assume $\boldsymbol{\mu}_q \in (0, 1]$ and $\sum_{q=1}^{Q_\lambda} \boldsymbol{\mu}_q \leq 1$. We used $x_0 = (0, 0, 365.76)'$, $\varepsilon = 83.82$, $Q_\lambda = 6$ and $\alpha_q \approx 128(q-1)$ in our example. In Figure 5.8 we display the mobility function for two choices of $\boldsymbol{\mu}$. Finally, we set $f \equiv 0$, $g_D = 0$ on $\Gamma_D = \{(x, y, z) \in \partial\Omega | y = 670.56\}$, $g_N = 1$ on $\Gamma_{N,1} = \{(x, y, z) \in \partial\Omega | y = 0\}$ and $g_N = 0$ on $\Gamma_{N,2} = \partial\Omega \setminus \Gamma_D \cup \Gamma_{N,1}$ to complete the problem definition. A typical fine DG solution of the SPE10 example is plotted in Figure 5.7 (bottom).

We compute our LRBMS approximation on different coarse triangulations consisting of $1, 2 \cdot 2 \cdot 2 = 8, 2 \cdot 4 \cdot 2 = 16$ and $4 \cdot 4 \cdot 2 = 32$ equally sized cubes. Figure 5.9 shows the evolution of the maximum estimated absolute error over the training set

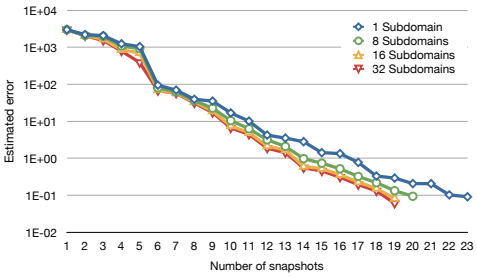

FIG. 5.9. *Maximum estimated absolute error over the training set against number of snapshots needed during Greedy algorithm for the different coarse triangulations.*

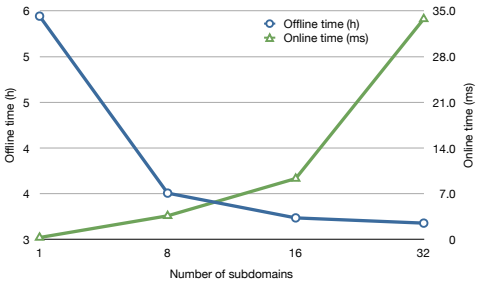

FIG. 5.10. *Offline time (snapshot computation, computation of reduced quantities and training time) and online time (time for one online simulation) against number of subdomains. Notice the different units of the ordinate axes.*

during the Greedy algorithm, the tolerance of which was set to $\Delta_{\text{error}} = 0.1$. Again the number of snapshots needed to fulfill the error tolerance decreases with increasing numbers of coarse elements. In this example, the decrease is not as big as in the thermal block example which is most certainly due to the larger spatial dimensions of the fine grid and smaller amount of coarse elements. Similar to the previous example, the estimator update times increase with the number of coarse grid elements: The mean time for one update rises from approximately 0.36 hours for 1 coarse grid element to 0.59 hours, 1 hour and 1.69 hours for 8, 16 and 32 coarse grid elements respectively. Again, this increase can be compensated by an efficient parallelization. Apart from the error estimator, our new scheme pays out for this test case: For 16 and 32 coarse elements we need 4 snapshots less than a standard RB method needs, which saves about 37 minutes of computation time during the offline phase. This effect can be seen nicely in Figure 5.10: With increasing numbers of coarse grid elements, the offline time (excluding the time needed to update the error estimator) drops from 5.4 hours to 3.46 hours while the online time rises from 0.3 milliseconds to 33 milliseconds. Note that here the offline time comprises times for snapshot computations as well as update times of the reduced operator and the training time, which is the time needed to compute the reduced simulations for all training parameters and to evaluate the error estimator for those reduced simulations.

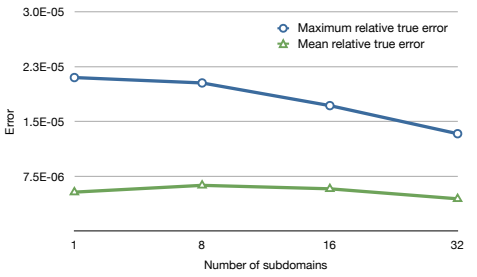

FIG. 5.11. *Mean and maximum relative true error (error between reconstructed reduced and detailed simulation) in the energy norm over the test set for different coarse triangulations.*

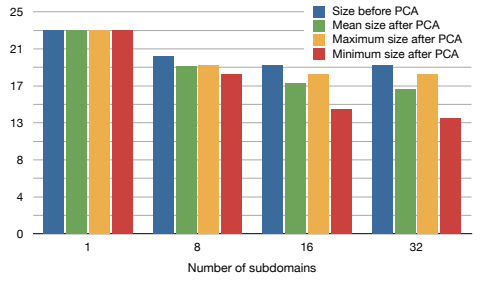

FIG. 5.12. *Mean, maximal and minimal local basis sizes for the different coarse triangulations before and after the PCA.*

In this case, the reduction of the offline time is not only due to the smaller amount of snapshots that need to be computed but also due to the faster projection of the high-dimensional quantities into the respective reduced spaces.

In Figure 5.11 we see an effect that we know from the previous example already: The maximum relative true error over a given test set decreases with increasing numbers of coarse elements. Here, the mean error stays at the same level. Although for this example the decrease in the error is not as decisive, it is worth noting that the approximation qualities of our scheme are better than those of a standard RB scheme.

Finally, similar to the previous example, we compare the effect of the PCA for the different coarse triangulations, this time using $\Delta_{\mathrm{PCA}} = 1 \cdot 10^{-4}$. In Figure 5.12 we observe the same behavior as for the thermal block example: With a rising number of subdomains, the difference between maximum and minimum numbers of basis functions on the different subdomains increases. We further see that although the Greedy algorithm needed 19 snapshots for both 16 and 32 subdomains to fulfill the error tolerance, the basis sizes after the PCA decreases.

6. Conclusions. In this paper we introduced the Localized Reduced Basis Multiscale method and demonstrated its applicability to heterogeneous elliptic multiscale problems. Depending on the choice of the coarse triangulation, this method interpolates between a standard DG method on a given fine triangulation and a classical RB approximation. Numerical experiments demonstrate that with this approach we are able to balance between offline and online cost depending on the multi-query scenario, always reaching a better online performance than a standard RB approach. While the proposed error estimator shows very pleasant performance for small coarse grid sizes, a more localized estimator is desirable for coarse grids with more subdomains.

Acknowledgments. Support by DFG Cluster of Excellence in Simulation Technology (EXC 310/1) and DFG-grant OH 98/4-2 is gratefully acknowledged.

REFERENCES

[1] J. E. Aarnes, Y. Efendiev, and L. Jiang. Mixed multiscale finite element methods using limited global information. *Multiscale Model. Simul.*, 7(2):655–676, 2008.

[2] M. Ainsworth and R. Rankin. Constant free error bounds for nonuniform order discontinuous Galerkin finite-element approximation on locally refined meshes with hanging nodes. *IMA Journal of Numerical Analysis*, 31(1):254–280, 2011.

[3] D. N. Arnold, F. Brezzi, B. Cockburn, and L. D. Marini. Unified analysis of discontinuous Galerkin methods for elliptic problems. *SIAM J. Numer. Anal.*, 39(5):1749–1779, 2001/02.

[4] M. Barrault, Y. Maday, N. C. Nguyen, and A. T. Patera. An empirical interpolation method: application to efficient reduced-basis discretization of partial differential equations. *Comptes Rendus Mathematique*, 339(9):667–672, 2004.

[5] P. Bastian, M. Blatt, A. Dedner, C. Engwer, R. Klöfkorn, M. Ohlberger, and O. Sander. A generic grid interface for parallel and adaptive scientific computing. part I: Abstract framework. *Computing*, 82(2):103–119, 2008.

[6] Z. Chen, G. Huan, and Y. Ma. *Computational methods for multiphase flows in porous media*, volume 2. Society for Industrial Mathematics, 2006.

[7] M. Drohmann, B. Haasdonk, and M. Ohlberger. Reduced basis approximation for nonlinear parametrized evolution equations based on empirical operator interpolation. *SISC*, 34(2):A907–A969, 2012.

[8] S. Kaulmann, M. Ohlberger, and B. Haasdonk. A new local reduced basis discontinuous Galerkin approach for heterogeneous multiscale problems. *Comptes Rendus Mathematique*, 349(23-24):1233–1238, December 2011.

[9] M. Ohlberger. Error control based model reduction for multiscale problems. In *Submitted to Algoritmy 2012, Conference on Scientific Computing, Vysoke Tatry, Podbanske, September 9-14, 2012.*, 2012.

[10] S. of Petroleum Engineers. SPE comparative solution project. Website. Information available online: http://www.spe.org/web/csp/.

[11] A. T. Patera and G. Rozza. *Reduced Basis Approximation and A Posteriori Error Estimation for Parametrized Partial Differential Equations.* 2008. Version 1.0, Copyright MIT 2006, to appear in (tentative rubric) MIT Pappalardo Graduate Monographs in Mechanical Engineering.

[12] K. Veroy, C. Prud'homme, D. V. Rovas, and A. T. Patera. A posteriori error bounds for reduced-basis approximation of parametrized noncoercive and nonlinear elliptic partial differential equations. In *In Proceedings of 16th AIAA computational fluid dynamics conference*, 2003. Paper 2003-3847.